Check for updates

Research Article | Vol. 32, No. 3 / 29 Jan 2024 / Optics Express 2972

Optics EXPRESS

Sub-wavelength scale characterization of on-chip coupling mirrors

V. V. TKACHUK,[1,*] J. P. KORTERIK,[1] L. CHANG,[2] AND H. L. OFFERHAUS[1]

[1] Optical Sciences Group, MESA+ Research Institute, University of Twente, The Netherlands
[2] Integrated Optical Systems Group, MESA+ Research Institute, University of Twente, The Netherlands
[*] v.tkachuk@utwente.nl

Abstract: Miniature free-space optical beams, originating from on-chip microstructures, are usually measured and quoted without reference to a particular polarization state. We develop an automated platform to characterize tightly focused free-space optical beams in three dimensions. We present a detailed description of each subsystem including the calibration and test procedure. We demonstrate how amplitude and phase are measured at sub-wavelength resolution using a cleaved fiber with a heterodyne reference. Further analysis provides information about the phase and intensity profile of the beam with regards to its polarization content and spatial confinement. We perform a proof-of-concept experiment for a custom waveguide-coupled micro-mirror. The work opens new possibilities for rapid analysis of micro-mirrors in prototyping and optimization of integrated optical systems.

© 2024 Optica Publishing Group under the terms of the Optica Open Access Publishing Agreement

1. Introduction

Over the past two decades, the number of produced photonic devices increased sharply. In particular, the fast development of 5G communications and autonomous vehicles drives the effort to create affordable optical signal processing solutions [1]. Novel methods of coupling light onto and out of a chip are developed by different research groups. With the emergence of these methods comes need for rapid and accurate characterization of the light coupling structures. For optical systems with microscopic dimensions, the electromagnetic field distribution is described both in terms of approximated Maxwell's equations and in terms of ray optics. Commonly, either the beam profile or the intensity and phase are measured for a given polarization state. Often times, while using non-ideal components, the optical beams represent a mix of rays of light with different polarization states and propagation characteristics. Generally, the free-space beams are described in terms of Gaussian beam optics by the beam size and curvature or the waist and Rayleigh range. The assumptions for these descriptions do not easily reflect mixed states that can be present therein. Measuring of the local optical phase and amplitude of the beams coming in and out of on-chip optical structures with an optical fiber provides a detailed understanding of the light beams.

1.1. *Coupling methods*

Inter-process testing plays an important role in cutting the production costs of Photonic Integrated Circuits (PICs) [2]. To test the optical properties of the PICs on wafer-scale, two popular coupling methods are: grating coupling and end-fire coupling [3]. Grating coupling is suitable for vertical coupling, but tends to have a relatively small bandwidth, typically a few tens of nanometers, especially in low contrast material platforms [4]. This method also requires a particular polarization of the incoming light. It can be used for rapid wafer-scale testing, but is unable to deliver a broad spectrum of wavelengths and polarizations, which is often a requirement in non-linear photonic applications [5]. End-fire coupling allows for broadband communication

#506358
Journal © 2024

https://doi.org/10.1364/OE.506358
Received 28 Sep 2023; accepted 26 Dec 2023; published 16 Jan 2024

Optics EXPRESS

with polarization preservation. It is mainly limited by a considerable difference in mode size of the typical waveguide and the typical optical fiber. The transition loss can be mitigated by tapering [6]. Obviously, one cannot use end-fire coupling for the vertical coupling, which is required in the testing of wafers that have not been diced yet. If the wafer under treatment consists of multiple chips with edge-emitting devices, deep trench etching with optimal sidewall properties is needed, which is challenging. Using mirrors to couple to waveguides in deep trenches is a recently proposed method, which combines benefits of end-coupling such as broadband functionality and arbitrary polarization operation with possibility of vertical coupling [7,8]. It is, however, an emerging solution, and prototyping of such mirrors requires careful study of the reflected beams. This paper is organized as follows. We describe the principle behind polarization-resolved detection and the setup. Then we describe the sample, the measurement process, the results, and compare them to other existing techniques. We conclude with the potential development prospective.

2. Methodology

2.1. Polarization-resolved heterodyne measurement of light beam

For the testing of PICs, it is important to be able to resolve the polarization states. P- and S-polarized light behave differently when incident at material interfaces and preservation of the polarization state on-chip is complicated by birefringince and angled reflections. Mechanical stress and thermal expansion can cause further instability. This, combined with typically small size of the beams and their relatively low intensity, creates a challenging task for inter-process beam characterization. Different methods are available for measuring polarization states, however, many require a collimated beam and normal incidence of the light [9]. One way to measure the state of polarization is to reference the signal against a reference light beam whose state is known and stable.

2.2. Setup

Here, we demonstrate a precise and stable system for measuring low-intensity beams of arbitrary polarization, divergence and incidence. The principle of optical heterodyne detection has been applied to weak optical signal detection and has been described extensively both on-chip [10], in fibers [11] and in free space [12]. Light coming from a laser is split in two equal arms (sample and reference) to form a Mach-Zehnder interferometer. The reference signal's frequency is shifted by 40 kHz acousto-optically to allow heterodyne detection. The scanning head is incorporated in the signal arm. After the beams are combined, the light is split in the orthogonal polarization components and measured by the corresponding detectors. Outside the observed structure, the light rays propagate freely and can be picked up with a cleaved fiber or a near-field probe with a sub-wavelength aperture, depending on the required resolution (Fig. 1), attached to a calibrated 3D-positioning system. This positioning system is based on a previously reported vertically-arranged photon scanning tunneling microscope [13]. Free-space light is is picked up by a fiber probe. The light typically contains a combination of polarization and phase states in the vicinity of the probe. By moving the tip in a certain plane, the beam is probed and a coherent image of the electric field profile is built. A core advantage of this technique lies in the ability to accurately measure the local behavior of the light waves on a (sub-)wavelength scale. It also allows for chip-scale non-contact testing of optical on-chip microstructures. The setup exhibits repeatable accuracy and is consistent in large-scale (stitched) measurements. The characterization process is fully automated, including the data collection and analysis. The setup achieves precise positioning of the fiber probe on chip-scale by combining fine positioning, using bi-morph piezo-actuators with coarse alignment using actuators with absolute positioning. These are calibrated by scanning an AFM calibration grid (Edge Scientific HS-20MG AFM XYZ

Optics EXPRESS

calibration standard). For the purpose of this research, the setup was outfitted with a three-axis sample positioning stage for coupling light in the chip.

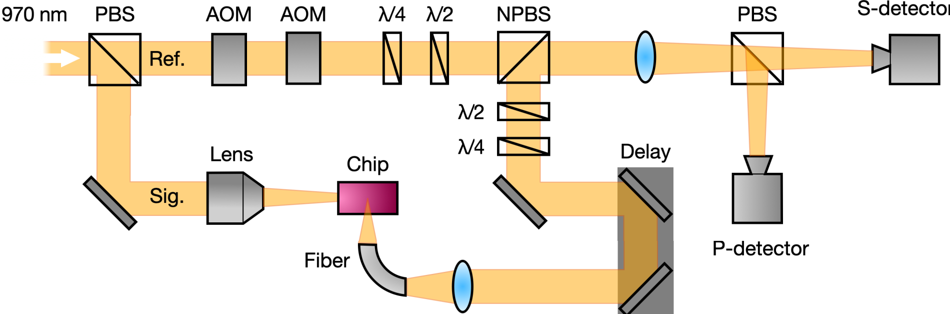

Fig. 1. Schematic representation of the setup.

A Toptica DL pro light source was operated at 970 nm and tuned for single-mode operation across different power levels. The light was coupled to the sample through a microscope lens using the three-axis piezoelectric stick-slip motor system of the sample mount and images captured by a camera (Allied Vision Guppy PRO F-146B), sensitive to both visible and near-infrared light, positioned coaxial to the in-coupling laser beam near the desired part of the sample. The image from this camera is also used to help with positioning the fiber probe with respect to the sample and to measure the separation between the fiber and the top of the structure (Fig. 2). Following that, a more accurate positioning was performed using the steering mirrors of the coming light and monitoring the amount of light detected by the tip of the fiber, which is later brought in close proximity to the observed structure at the desired location. This setup demonstrated the potential for wafer-scale optical metrology, which, to the knowledge of the authors, was not published before.

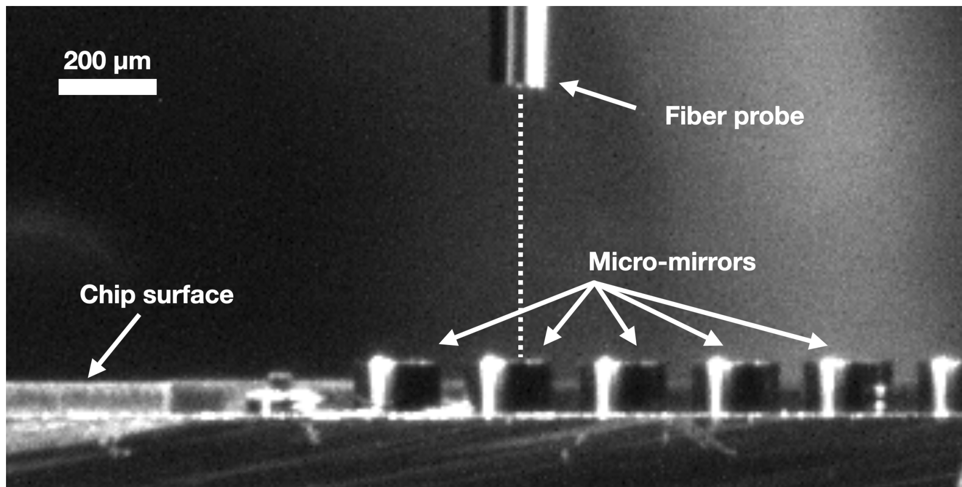

Fig. 2. Microscope image of the sample and fiber probe (side view). The dashed line marks the path of the observed light beam.

Optics EXPRESS

2.3. Sample

Figure 3 shows the layout of the fabricated device, consisting of a clad waveguide with two S-bends and a micro-mirror aligned to one end of the waveguide. The parameters of the waveguide are: thickness 200 nm, width 1.3 µm, total length 10 mm, waveguide side-wall angle 65 deg. At the end facing the mirror, the waveguide tapers down to the width of 150 nm for better coupling. The device is fabricated on a thermally oxidized silicon wafer on which 200 nm LPCVD Si_3N_4 layer was deposited. Structures were defined using electron beam lithography, followed by reactive ion etching to transfer the pattern into the substrate. The finished waveguides are clad with 6 µm SiO_2. A 1 mm wide, 60 µm deep trench is etched near the waveguide to accommodate the mirrors. Two objects per waveguide are produced via two-photon polymerization (Nanoscribe Photonic GT): a cap and a mirror. The cap shields the end facet of the waveguide from aluminum deposition. The mirror reflects the light coming from the waveguide vertically. Its positioning relative to the waveguide is done by alignment of the printing position relative to the optical image of the chip. 50 nm of Al is deposited at a slanted angle, and the excess is etched in a custom formulated solution by partially dipping the chip.

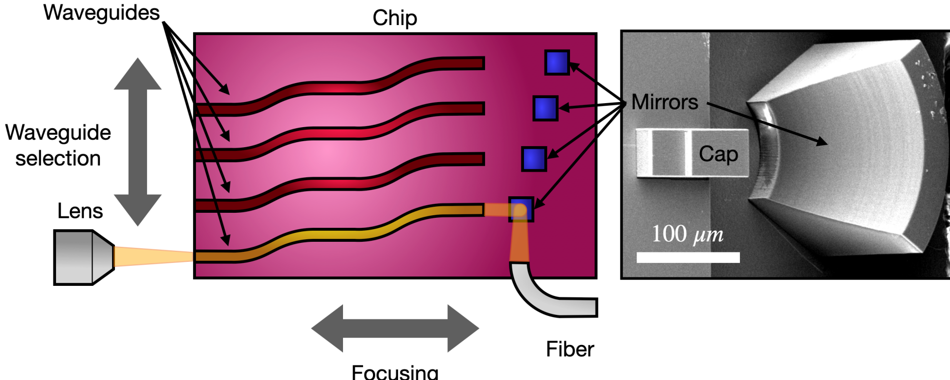

Fig. 3. Schematic representation of the experiment on measuring the free-space beam originating from the on-chip printed micro-mirror. Right insert: SEM image of one of the mirrors on the chip (adopted from [7] with permission). Note that the alignment is preserved with respect to the waveguide, but only the cap is visible on SEM image.

The expected mode profile of the waveguides was analytically determined using experimental data obtained for similar devices produced in the same process on the same equipment. The fundamental TE mode has an effective group index of 1.53 at 970 nm. A far-field simulations was carried out to estimate the beam profile coming out of the waveguide (Ansys Lumerical). The planar far field was estimated to be circular, with both TE and TM modes having FWHM of 5.8 µm at 20 µm from the end facet, and 22 µm at 100 µm from the end facet. An Ansys Lumerical Finite Difference Eigenmode (FDE) simulation was carried out with the characteristics of the waveguide, obtained during the fabrication. The focused spot diameter is estimated to be 9.6 µm FWHM with a Rayleigh range of 74 µm, and a divergence half-angle of 3.7°. The fiber probe is used to measure amplitude and phase images of the reflected light following the procedure described in **Supplement 1**. The fiber tip is scanned across an area of 70×70 µm. Several in-plane areas were scanned, as well as a series of height-stacked areas. The complex amplitude images are used for reconstruction of the light field in the spatial domain and spatial-frequency domain, as shown in Fig. 4. The results in Fig. 7 show that the propagating light is reflected by the mirror, together with stray light carried by the cladding. The lock-in detection of the heterodyne interference produces electric field amplitude and phase information for each polarization, as received by the corresponding detector. The exact mechanism of heterodyne detection is described in detail in

[11]. The signal from the waveguide contains only one polarization, because of how the light was coupled in the system. The intensity picture was generated by computing the length of the complex amplitude vector, and the phase picture was generated by calculating the angle of it which is unwrapped to create a continuous image.

Table 1. FWHM measurement at several positions above the top surface of the examined micro-mirror.

No. scan	FWHM X, μm	FWHM Y, μm	Height, μm
1	34.5	25.8	191
2	41.3	26.6	291
3	47.6	28.2	391
4	51.3	30.7	491
5	56.0	34.0	591

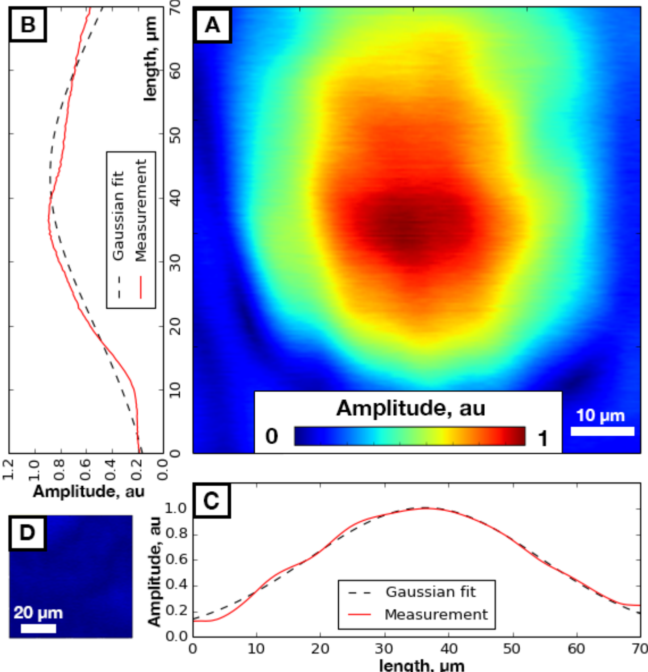

Fig. 4. A – Example measurement of the amplitude of a free-space beam. The sub-graphs (B, C) illustrate the averaged section in X- and Y-axes against the fitted Gaussian function. D – the detected amplitude on the second detector (same intensity pseudo-color as A).

Optics EXPRESS

3. Model, analysis and calibration

The wave-plates in the signal arm compensate for the birefringence of the fiber probe (Fig. 5). First we measure the input beam separately by placing a polarizing beam-splitter (PBS) that reflects the light vertically. The fiber is brought in the path of the beam and the interference signal on the detectors is used to align all the waveplates in the signal arm to maximize the signal on one of the detectors. The other detector therefore receives the orthogonal polarization only.

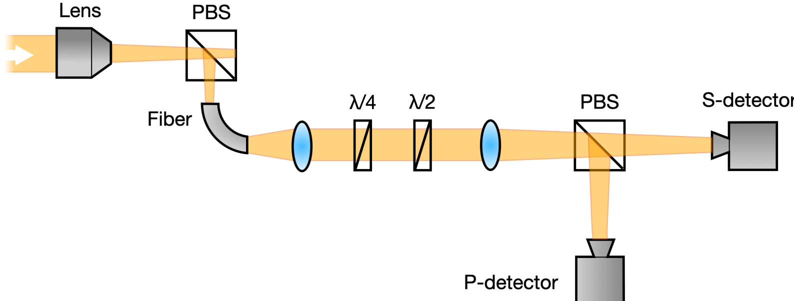

Fig. 5. Schematic representation of the part of the setup that is changed for aligning the wave-plates.

3.1. Measurement procedure

The sample is mounted onto a vacuum-holding chuck and is coarsely aligned with respect to the waveguide tapers and the in-coupling lens. The laser spot is positioned on the side of the chip by coarse manual adjustment, and is observed by a infrared-sensitive digital camera. The chip is then moved on its stage in and out of the focus of the in-coupling lens (20×, with B-type coating) until the spot size is minimal. The focused spot diameter is ≈ 10 μm, as estimated by an optical image, which is larger than the waveguide mode size is, to achieve coupling stability over a typical scanning time of a few hours. This mismatch, however, yields a substantial amount of stray light in the cladding, which has an influence on some of the measurements. Then the chip is aligned in the vertical and horizontal direction until the spot is near the waveguide taper. Because the sample has a relatively thick cladding, the light can be directly observed propagating inside it due to scattering. The camera lens is adjusted using this light. Fine adjustment is done by both piezo stick-slip motors and by manual adjustment of the mirrors that are steering the light in the in-coupling lens. Lateral movement of the chip perpendicularly to the optical axis allows selecting different waveguides. Then the camera is adjusted on the mirror adjacent to the selected waveguide. The beam is again finely aligned by manual adjustment of the mirrors to minimize light on neighbouring mirrors to minimize possible interference resulting from picking light from several mirrors at the same time by the fiber probe.

The fiber probe is coarsely positioned on top of the mirrors, guided by the microscope image. At a safe distance of ≈100 μm above the mirror surface, the abundance of signal across a wide area allows for coarse and fine positioning of the fiber by maximizing the intensity of the optical signal on the detectors. A wide-area scan can be captured (Fig. 8). It is usually immediately evident where the brightest spot is in the mix of light reflected from the waveguide and stray light, reflected from the other components in the setup. This results in an indeterminate mix of polarization between two channels. After that, the fiber is vertically raised by 1-3 mm, and the scan area is aligned with the brightest spot in the center. At this height, the near field light and other higher-order modes are extinct, and only the propagating beam is present. For a single polarization input, all the light beam should fall on one detector, while the unwanted reflections and possible interference from the other mirrors are limited to the other detector.

Optics EXPRESS

Finally, the length of the reference branch and signal branch can be equalized by moving the delay line of the signal branch while monitoring the interference the on the lock-in amplifiers and frequency tuning the laser; when the path lengths are equal, the interference becomes independent of the frequency tuning.

After that, the setup is interferometrically stable for several days, and measurements can be taken in an automated manner where each scan file is supplemented by a list of coordinates and other parameters for the analysis.

4. Results

4.1. Beam investigation

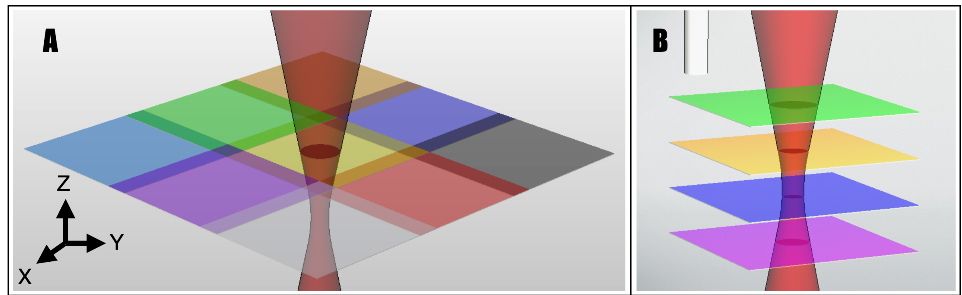

Fig. 6. Different ways of stacking multiple scan fields. A - lateral stacking of overlapping fields. B - vertical stacking of the fields, centered on the beam. Combination of A and B is also easily realized.

Scanning is done in several fields stacked either laterally or horizontally (Fig. 6). This allows for measuring wide beams, or several smaller beams. Beam quality is often expressed using the M^2 value which is a measure for the brightness of the beam and therefore a combination of the spatial extent and the angular content. A lowest order single mode beam as an M^2 value of one in both directions perpendicular to the propagation direction. The M^2 value scales as $(2n + 1)$ with the mode order number n. There are two approaches to measuring the beam quality (M^2) value. One requires taking several measurements both in and outside the focal plane of the beam and is described in detail in ISO Standard 11146 [14]. The other one requires only a single measurement if the complex amplitude (amplitude and phase) of the electric field is measured [15]. With the full complex information the angular composition can be obtained from the intensity distribution of the (complex) Fourier transform of the fields and the widths in real space and angular space can be combined to obtain the M^2 value. For the case of scanning the PBS (Fig. 5) we can directly compare the conventional measurement protocol with single measurement technique, and they come out to approximately the same value ($M_x^2 \approx 4, M_y^2 \approx 6$). This is larger than expected for a single mode beam due to a partial reflection that is co-propagating. From these measurements it is clear that both methods generate the same result (Table 1) and the half-angle of divergence can be estimated to be around 3.04° in X-direction and 1.19° in Y-direction. While scanning the waveguide-coupled mirror, the conventional protocol for estimating M^2 cannot be implemented because, due to lack of focusing lens between the waveguide and the mirror, the beam is diverging, and this divergence angle is preserved by the mirror. Thus only the single-shot measurement is applicable. The resulting scan image contains the main beam (as seen by the peak value of intensity) corresponding to the initially launched S-polarization, as well as one beam in P-polarization which can clearly be traced to unwanted reflections from the sides of the polarizing beam splitter cube. Note that these figures are far from a perfect Gaussian shape. One of the reasons as to why is that the waveguide and mirror are not designed for this wavelength.

There are several beams present on the image, most likely due to unwanted reflections on the chip. Importantly, the separation of the polarizations allows us to gain insight which beams are of the same polarization. The difference in signal-to-noise-ratio between the intensity and heterodyne measurement is also obvious.

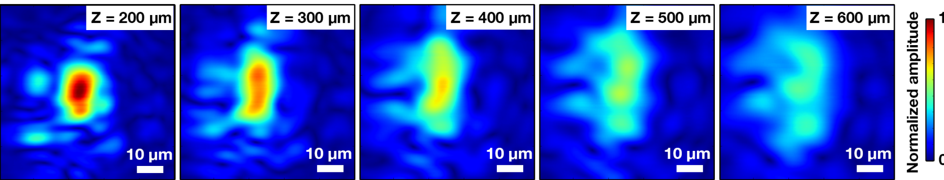

Fig. 7. Scan images for dominant S-polarization of the beam as measured over the printed mirror. A-E correspond to aligning the scan fields as demonstrated in Fig. 6, B. The information from this scan is used to compose Table 1.

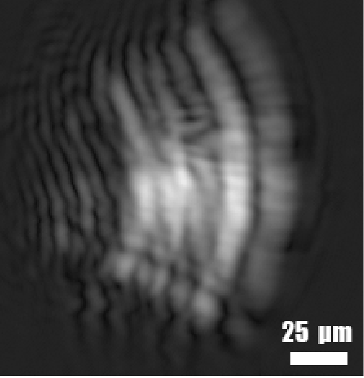

Fig. 8. An example of laterally stitched image. Each image corresponds to aligning the scan fields as demonstrated in Fig. 6, A.

Additionally, from the position of the center of the scanned beam with respect to the scanned area, we can calculate the angle of inclination of the beam of 0.43° with respect to the X-axis and 3.21° with respect to Y-axis.

5. Discussion

Depending on the type of the light beam under treatment, two approaches may be considered. If the beam has a focus and waist, it is possible to use the method described in ISO Standard 11146, and produce minimum of 5 scans in the beam waist, as well as 5 scans beyond 2× Rayleigh lengths. A collimated or diverging beam may also be characterized in this manner, but it requires using an additional component, an aberration-free lens, to produce focus. This fact, however, may reduce the convenience and fidelity of the measurement. This method also requires stability of the system in the time that is needed for re-positioning of the measurement device, and thus is sensitive to drift. Furthermore, either a fixed beam profiler with a CCD matrix, or a pinhole or slit-type scanning beam profiler can be used to quantify the content of the beam. Both methods have their advantages and disadvantages, for example, the former can resolve short pulses and discern between complex beam profiles, but it struggles with small beams relative to the resolution, while the latter can resolve microscopic beam, but cannot resolve the exact shape of the beam, and is limited in its measurement time. Using complex amplitude

Optics EXPRESS

of the E-field to measure the beam quality allows direct single measurements at virtually any plane in the beam propagation, independent of the degree of collimation. Using the optical fiber (optionally with a sub-wavelength aperture) for probing the beam locally, combined with heterodyne detection, allows to measure low-power microscopic beams with sub-wavelength spatial resolution, thus providing benefits of both comparable methods, and provides information about present polarization in the beam. Ability to scan at several desirable distances from the structure allows for both conventional and phase-resolved M^2 beam quality measurements.

6. Conclusion

We have demonstrated phase- and polarization-resolved measurement of a complex and distorted light beam. We can use the M^2 value to quantify the quality of the beam from the amplitude and phase of the beam, even if it is divergent, and the conventional method of measuring M^2 is not attainable. Moreover, by introduction of precise fiber positioning, we can characterize the light in the vicinity of the chip, with minimal sample-probe separation on the order of micrometers, which provides an advantage compared to CCD-based beam characterization. Moreover, as the resolution is not limited to the physical size of an imaging pixel, but to the effective diameter of the probe, the resolution far surpasses the conventional beam quality analyzers. Presence of Mach-Zehnder interferometer in the optical part of the setup enables heterodyne detection without compromising the flexibility of measurements enabled by the principles of probe microscopy. These advantages distinguish the described setup and measurement technique among the other known methods of polarization-resolved analysis of miniature free-space optical beams in on-chip microstructures.

Acknowledgments. The authors thank Y. Kong and M. Dijkstra (Optical Sciences group, MESA$^+$ research institute, University of Twente) for providing the sample for analysis.

Disclosures. The authors declare no conflicts of interest.

Data availability. Data underlying the results presented in this paper are not publicly available at this time but may be obtained from the authors upon reasonable request.

Supplemental document. See Supplement 1 for supporting content.

References

1. "Photonics roadmap," (2023). https://photonicsmanufacturing.org/, accessed: 13.09.2023.
2. M. Trappen, M. Blaicher, P.-I. Dietrich, *et al.*, "3d-printed optical probes for wafer-level testing of photonic integrated circuits," Opt. Express **28**(25), 37996–38007 (2020).
3. M. M. Milosevic, X. Chen, W. Cao, *et al.*, "Towards autonomous testing of photonic integrated circuits," Proc. SPIE **10108**, 1010817 (2017).
4. A. Mekis, S. Gloeckner, G. Masini, *et al.*, "A grating-coupler-enabled cmos photonics platform," IEEE J. Sel. Top. Quantum Electron. **17**(3), 597–608 (2011).
5. C. R. Doerr, L. Chen, Y. K. Chen, *et al.*, "Wide bandwidth silicon nitride grating coupler," IEEE Photonics Technol. Lett. **22**(19), 1461–1463 (2010).
6. C. Hu, A. Pan, T. Li, *et al.*, "High-efficient coupler for thin-film lithium niobate waveguide devices," Opt. Express **29**(4), 5397 (2021).
7. L. Chang, M. Dijkstra, N. Ismail, *et al.*, "Waveguide-coupled micro-ball lens array suitable for mass fabrication," Opt. Express **23**(17), 22414 (2015).
8. Y. Kong, H. Offerhaus, M. Dijkstra, *et al.*, "3d printed on-chip parabolic mirror for chip-to-fiber and chip-to-chip coupling," in *ECIO 2022: 23rd European Conference on Integrated Optics*, (Politecnico di Milano, 2022), pp. 324–326. 23rd European Conference on Integrated Optics, ECIO 2022, ECIO ; Conference date: 04-05-2022 Through 06-05-2022.
9. T. Käseberg, J. Grundmann, T. Siefke, *et al.*, "Mueller matrix ellipsometric approach on the imaging of sub-wavelength nanostructures," Front. Phys. **9**, 819 (2022).
10. E. Schipper, A. Brugman, C. Dominguez, *et al.*, "The realization of an integrated mach-zehnder waveguide immunosensor in silicon technology," Sens. Actuators, B **40**(2-3), 147–153 (1997).
11. M. L. M. Balistreri, H. Gersen, J. P. Korterik, *et al.*, "Tracking femtosecond laser pulses in space and time," Science **294**(5544), 1080–1082 (2001).
12. H. Gersen, "Time resolved motion of pulses in photonic crystal waveguides: a real space investigation," Ph.D. thesis, University of Twente, Netherlands (2004).

Optics EXPRESS

13. J. Jose, F. B. Segerink, J. P. Korterik, *et al.*, "Near-field observation of spatial phase shifts associated with Goos-Hänschen and Surface Plasmon Resonance effects," Opt. Express **16**(3), 1958 (2008).
14. ISO/TC 172/SC 9, "Lasers and laser-related equipment — Test methods for laser beam widths, divergence angles and beam propagation ratios — Part 1: Stigmatic and simple astigmatic beams," 2nd ed. (2021).
15. H. Offerhaus, C. Edwards, and W. Witteman, "Single shot beam quality (m2) measurement using a spatial fourier transform of the near field," Opt. Commun. **151**(1-3), 65–68 (1998).

130.89.110.190 {ts '2024-02-22 03:56:26'}